Temperature and density dependence of the shear viscosity of liquid sodium

N. Meyer, H. Xu, and J.-F. Wax[*]

Laboratoire de Chimie et de Physique - A2MC, Université de Lorraine - Metz, 1, boulevard Arago 57078 Metz Cedex 3, France

The density and temperature dependence of the shear viscosity of liquid sodium is studied. The stress autocorrelation function is calculated by equilibrium molecular dynamics simulations, which allow us to obtain the value of shear viscosity using the Green-Kubo formula. The Fiolhais potential is used to calculate the interionic interactions, which are validated by comparison between simulation and experimental data along the liquid-gas coexistence curve. The behavior of viscosity over a wide range of the liquid phase of the phase diagram is studied. Along isochoric lines, it presents a minimum, while it monotonically increases along isotherms. An expression is proposed for the viscosity as a function of temperature and density which reproduces our data for liquid sodium at any density in the range [1000–2000 kg m^{-3}] and any temperature in the range [700–7000 K]. The validity of the Stokes-Einstein relation over the investigated state points is discussed.

I. INTRODUCTION

Liquid metals play an important role in several fields. Their main characteristics are high electrical conductivity, boiling temperature, latent heat, specific heat, thermal conductivity and diffusivity, as well as low viscosity. This latter property is relevant for several purposes, and first of all in metallurgy to control casting. In geophysics, the viscosity of materials in the Earth's core allows us to determinate the properties of the core itself [1], such as core convection responsible for the magnetic field of our planet [2]. However, even its estimate has been the subject of debate as it spans more than 12 orders of magnitude [3,4]. In this context, the fluid is subject to high pressures [5] and the study of the viscosity versus density is necessary. In cooling systems, the low viscosity value, of the same order of magnitude as other common fluids such as water, permits us to pump liquid metals through tubes and heat exchangers at a reasonable cost. A knowledge of temperature behavior of the viscosity is then essential to improve many industrial processes. As a last example, having high electrical conductivity and low viscosity, they are excellent candidates to carry out electric connections through microtubes in flexible electronic devices [6].

Among liquid metals, sodium has a certain technological interest. It could be used as heat transfer fluid within the new generation nuclear reactors [7]. Indeed, while water requires several hundreds of bars to remain liquid at temperatures over 100 °C, sodium remains liquid up to 900 °C under atmospheric pressure. Moreover, liquid sodium has a viscosity lower than water (typically about 10^{-3} Pa s) which is favorable to industrial use.

Despite the technological interest of sodium, experimental studies of its viscosity are very limited and date back to the 1960s or earlier [8–11]. Moreover, data are restricted to a relatively small temperature range and only under atmospheric pressure. This is first due to the high chemical reactivity of alkali metals which adds to the difficulty in comparison with other metals. Second, the very low viscosity value requires very careful measurements and implies high uncertainty. The usual method consists of measuring the damping of an oscillating

crucible filled with liquid metal [12]. As a consequence, the available experimental data have not been updated for decades. Furthermore, measuring the viscosity of sodium under high pressure or at high temperature is nearly impossible in this context.

Conversely, numerical simulation permits the prediction of some properties over a wide range of thermodynamical states. Transport coefficients such as viscosity can be obtained from correlation functions using the Green-Kubo relation. It involves the stress autocorrelation function (SACF) which is computed from microscopic configurations generated by molecular dynamics (MD) simulations. Being a collective property, the computation of viscosity requires a rather long simulated time in order to improve statistical accuracy. Therefore, classical MD should be favored instead of *ab initio* ones which are more accurate, but much more demanding from the computation time point of view. Curiously, to our knowledge, there is no complete study of the dependence of viscosity with temperature or density available in the literature for any liquid alkali metal. We can mention Refs. [13] and [14] which both deal with sodium only along the liquid-vapor coexistence curve, the second one having used nonequilibrium MD.

To perform classical simulations, a realistic description of the interactions is required. This is *a fortiori* true in the case of metals as the interactions strongly depend on density. As sodium (like other alkali metals) is considered as a simple metal because it only has one valence electron, its electronic structure is rather simple and there exist interatomic pair potentials which can accurately describe its behavior. The potential of Fiolhais *et al.* [15] initially developed for the solid state has proven its capability to describe the alkali metals in the liquid state. According to Refs. [16–19] (and references therein), this potential has demonstrated a very good ability to predict the static structure, diffusion coefficient, and dynamic structure factor for all the alkali metals and some of their alloys over a wide range of thermodynamic states. So, the Fiolhais potential has been chosen for our simulations.

In this study, we will first compute the viscosity of liquid sodium at thermodynamic states where experimental data are available, i.e., at ambient pressure to confirm the reliability of the description of the interactions. These states are close to the liquid-vapor coexistence, and we will extend the study to

---
[*]Corresponding author: jean-francois.wax@univ-lorraine.fr

very high temperatures (up to 7000 K) and densities (up to 2000 kg m^{-3}). Such a wide region of the phase diagram will allow us to discuss separately the dependence on temperature and density and to propose an empirical expression of viscosity over this wide phase diagram part. We will also compare the behavior of this liquid metal to Lennard-Jones fluid where interactions are independent of the density. Finally, the validity of the well-known Stokes-Einstein relation binding the viscosity and self-diffusion coefficient of a liquid will be examined.

This paper is laid out as follows. Section II is devoted to the description of the interaction potential and to a presentation of the sodium phase diagram. Indeed, the metallic nature of sodium depends on the state point. We also give relevant computational details in order to obtain the shear viscosity from the SACF. In Sec. III, the results of shear viscosity are analyzed and compared with experimental data available in the literature. The temperature and density dependence is also discussed and our empirical expression is proposed. The validity of Stokes-Einstein relation between viscosity and diffusion coefficient is discussed. Finally, in Sec. IV we give the conclusions and the perspectives of this work.

II. FORMALISM

A. Interaction description

In simulations, the crucial point is the description of the interactions as it will condition the realism of the predicted behavior of the system. For alkali metals and therefore sodium, a density-dependent effective pair potential derived from the Fiolhais model [15] of electron-ion interaction and from self-consistent screening using the local field correction of Ichimaru and Utsumi [20] has shown good ability to reproduce the static and dynamic structures, as well as atomic diffusion properties. Although it was initially developed for the solid state, it is also accurate for the liquid along the liquid-vapor coexistence curve and for alloys of alkali metals. Its expression, namely,

$$u(r) = \frac{Z^2}{r} \left\{ 1 - \frac{2}{\pi} \int_0^\infty F_N(q) \frac{\sin qr}{q} dq \right\}, \quad (1)$$

comprises a direct Coulombic repulsion between ions of valency Z plus an indirect attraction involving the electron gas. This last term is expressed using the energy-wave number characteristic

$$F_N(q) = \left(\frac{q^2}{4\pi} \right)^2 \frac{1}{Z^2} w^2(q) \left[1 - \frac{1}{\varepsilon(q)} \right] [1 - G(q)], \quad (2)$$

accounting for the electron-ion interactions [$w(q)$, Fiolhais potential] and the electron-electron contribution [$\varepsilon(q)$ and $G(q)$, screening functions]. Complete analytical expressions, as well as references to earlier studies, can be found in Ref. [17].

Some important features of metallic potentials should be recalled. The first one is that they are density dependent (Fig. 1). This could influence the density dependence of the physical properties of the system when compared to fluids like Lennard-Jones for instance. The second one is that the expressions above presuppose the existence of an electron gas, i.e., that the system is metallic. It is well established that alkali
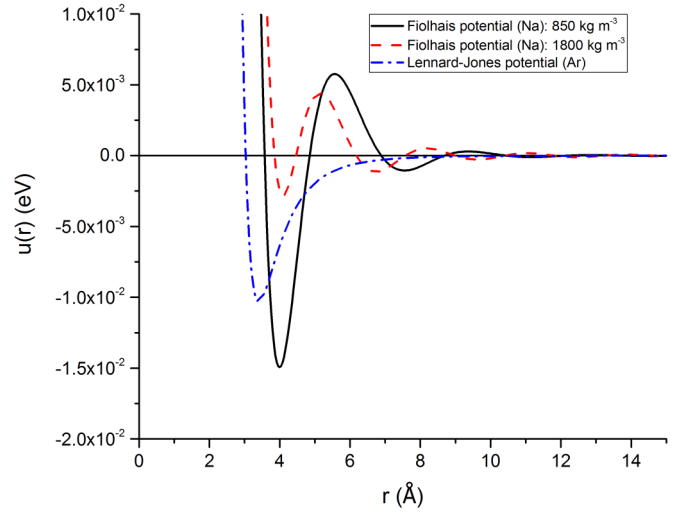
FIG. 1. Interaction pair potential for sodium at two densities, namely 850 kg m^{-3} (solid black line) and 1800 kg m^{-3} (dashed red line), compared to Lennard-Jones potential for argon (dash-dotted blue line).

metals undergo a metal-to-nonmetal transition at about twice the density of the critical point (namely $\rho_c = 230$ kg m^{-3} for sodium). Below this density, the material is no longer metallic and the description of the interactions used no longer valid. Therefore, we will not investigate thermodynamic states under this limit. On the other hand, temperature does not affect the interactions.

As mentioned in the introduction, the accuracy of the Fiolhais model of interaction has already been ascertained in the liquid state from the melting point at ambient pressure down to densities corresponding to the metal-to-nonmetal transition along the liquid-gas coexistence. Moreover, this model was developed for the solid state, and especially in order to render the correct bcc structure at ambient pressure conditions. Its ability to describe the interactions under high-pressure conditions will be discussed in the next section.

B. Phase diagram

The phase diagram of sodium is presented in the (ρ, T) plane in Fig. 2, as well as each state point studied in this work, with T, the temperature, and ρ, the density. As will be explained, these variables are convenient in the framework of molecular dynamics simulations. When available, we also indicate the pressure.

This complete phase diagram (low and high pressures) results from a compilation of literature data available for sodium [7,21–23]. These data were obtained either experimentally or by *ab initio* simulation methods. The solid, liquid, and gas phases are separated by solid lines. While the liquid-gas coexistence range is well determined and represented in this figure, we have no information on liquid-solid and solid-gas coexistence. Thus, the corresponding transitions are only approximately known.

As the pressure increases, solid sodium undergoes a structural transition from a body-centered b (bcc) to a face-centered-cubic (fcc) crystal at a density about 2300 kg m^{-3}. A
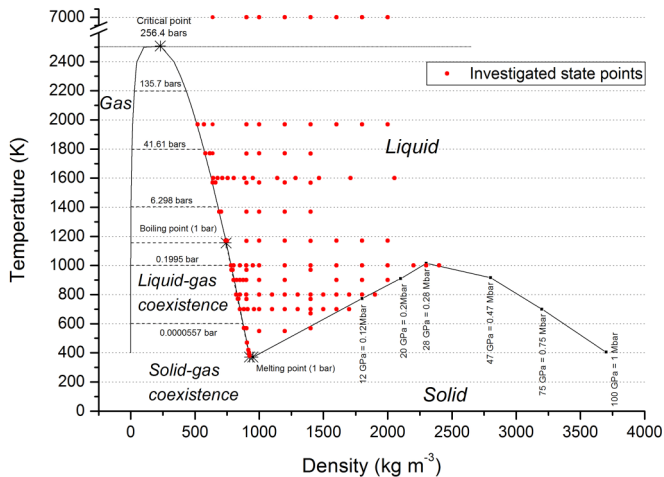
FIG. 2. Phase diagram of sodium. Red dots correspond to the investigated state points. Solid black lines delimit transitions between two different phases. Pressures are indicated when available.

FIG. 3. Evolution of the pair distribution function from the solid to the liquid phase at density 1800 kg m^{-3}. Lines: Our results with the Fiolhais potential; circles: *ab initio* results of Yamane *et al.* [21]. Inset: Corresponding mean-squared displacements.

pressure-induced drop of the melting temperature from 1000 K at approximately 30 GPa down to room temperature at more than 100 GPa was predicted by simulation [24] and confirmed experimentally [25]. At higher densities and pressures (not presented here), the temperature of liquid-solid transition is thought to increase again and solid sodium is thought to undergo further transitions to more exotic structures, but this is out of the scope of our study.

On the low-density side of the diagram, the critical point of the liquid-gas coexistence is located at density $\rho_c = 230$ kg m^{-3} with $P_c = 256.46$ bars and $T_c = 2508$ K. Under atmospheric pressure, the density at a given temperature is determined from the expression of Lucas [26]:

$$\rho = 0.927 - 2.23 \times 10^{-4}(T - T_m), \qquad (3)$$

where $T_m = 371$ K is the melting temperature under normal pressure. Along the coexistence curve, as given by Shpilrain *et al.* in Ref. [27] (Chap. 6.3.3, p. 453), the density at each temperature is given by the following relation, valid up to 2200 K:

$$\rho = \sum_{i=0}^{m} a_i \tau^i, \qquad (4)$$

where ρ is the mass density in kg m^{-3}, $\tau = T/1000$ with T the temperature (in K), and a_i parameters given in Ref. [27] (Chap. 6.3.3, p. 459).

All our simulations were performed at densities higher than $2.5\rho_c$, in order to avoid the metal-to-nonmetal transition. We investigated state points at temperatures ranging from the melting curve up to 7000 K and densities ranging from the liquid-gas coexistence limit up to the solidification curve or up to 2000 kg m^{-3}, if possible. According to Raty *et al.* [22], liquid sodium remains free-electron-like below this limit (about 40 GPa), so that we should not be faced with semimetal or semiconducting behavior. The liquid or solid nature of each state was checked by considering the pair distribution function, $g(r)$, and the mean-squared displacement. In order to estimate the reliability of the interaction description in the high-density range, we have plotted in Fig. 3 the evolution
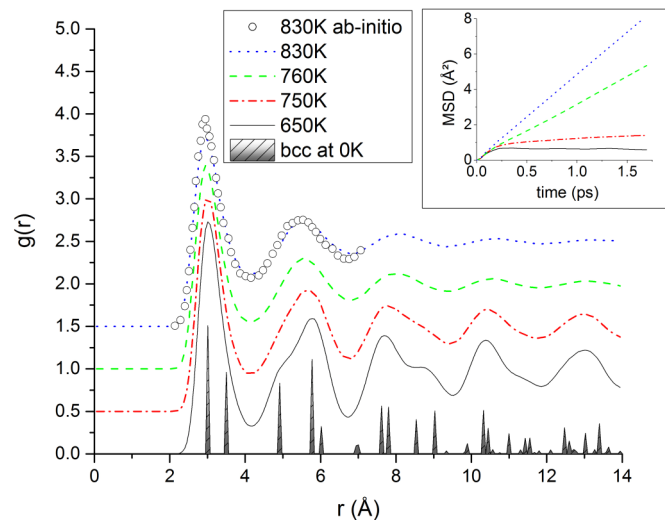
of the pair distribution function $g(r)$ and of the mean-squared displacement along the isochoric line corresponding to density 1800 kg m^{-3}. Starting from a bcc solid, the temperature was increased in a "heat until it melts" approach in order to estimate the stability of the liquid phase. At each temperature, the thermalization stage lasted 10 000 time steps and the production stage 50 000. Although overheating of the solid phase is possible, we observe melting between 750 and 760 K, in agreement with the phase diagram. Furthermore, our predicted structure compares favorably with *ab initio* results [21] in the liquid phase at 830 K.

We consider that this is an indication of the reliability of the Fiolhais potential, even in this high-density range. To our knowledge, there is no previous work investigating the predictions of this potential under high pressures; this may be the subject of another study in the future.

C. Molecular dynamics

Our simulations were carried out in the NVE ensemble, also called microcanonical, which consists in keeping constant the number of particles, N, the volume, V, and the total energy, E. Our simulations were performed with 2048 particles in a cubic box of side L and initialized with an fcc structure, i.e., an $8 \times 8 \times 8$ repetition of a four-atom primitive cell of the fcc lattice. This number of particles appeared large enough to limit the temperature fluctuations [28] and the finite-size effect on the viscosity as will be explained later. Verlet's algorithm in its velocity form was used to compute the positions and velocities of each particle, implementing the usual periodic boundary conditions and minimum image convention in the three directions [29]. The interaction cutoff radius was chosen at the node of the force directly inferior to $L/2$, in order to limit truncation errors.

The time step was chosen in order to avoid significant temperature drift (typically, $\Delta t = 0.37$ fs). During the thermalization stage lasting at least 50 000 steps, the velocities

were rescaled every 50 time steps to the expected temperature. This allows the system to relax and to reach the desired (T, ρ) state point. Then, during the production stage, velocities were left free to evolve and configurations were recorded every 10 time steps. In order to reach the required accuracy when computing the viscosity, this stage lasted typically 1 ns, that is, about 3 000 000 steps. At some given state points, it was necessary to decrease the time step value in order to assure that the temperature remains stable during such a long simulation. When this was necessary, the number of time steps was adjusted to keep the simulated time equal to 1 ns. In any event, the temperature drift was less than 4.0% (and most of the time less than 2.0%), which is smaller than the temperature fluctuations in the NVE ensemble.

D. Viscosity

The shear viscosity, η, corresponds to the resistance of a fluid to shear forces. It can be obtained thanks to the Green-Kubo expression by integration of the time-autocorrelation function of the off-diagonal elements of the stress tensor:

$$\eta = \frac{V}{k_B T} \int_0^\infty \langle \delta\sigma_{\alpha\beta}(0)\, \delta\sigma_{\alpha\beta}(t) \rangle dt, \tag{5}$$

where V is the volume of the system and T its temperature, k_B is the Boltzmann constant, and $\sigma_{\alpha\beta}$ the $\alpha\beta$ component of the stress tensor (with $\alpha, \beta = x, y, z$) [29]. The notation $\langle \cdots \rangle$ refers to an average over a sufficiently large number of phase-space trajectories in order to reach the thermodynamic mean, and $\langle \delta\sigma_{\alpha\beta}(0)\, \delta\sigma_{\alpha\beta}(t) \rangle$ is called the stress autocorrelation function (SACF). For a system of N particles in volume V at equilibrium, the stress-tensor elements $\sigma_{\alpha\beta}$ read

$$\sigma_{\alpha\beta} = -\frac{1}{V}\sum_{i=1}^{N} m_i (\mathbf{v}_i)_\alpha (\mathbf{v}_i)_\beta - \sum_{i=1}^{N-1}\sum_{j>i}^{N} (\mathbf{r}_{ij})_\alpha (\mathbf{f}_{ij})_\beta + \sigma_{\alpha\beta}^{(0)}(\rho, T)$$

$$= \delta\sigma_{\alpha\beta}(t) + \sigma_{\alpha\beta}^{(0)}, \tag{6}$$

where $\mathbf{r}_i$, $\mathbf{v}_i$, and m_i are respectively the position, velocity, and mass of particle i, and $\mathbf{r}_{ij} = \mathbf{r}_i - \mathbf{r}_j$ and $\mathbf{f}_{ij}$ are the relative coordinates and pair forces between two particles i and j; $\sigma_{\alpha\beta}^{(0)}$ is a contribution specific to liquid metals depending on T and ρ, but not on time [30].

In Eq. (5), the viscosity η is computed with a finite upper limit $t_{\max}$ in the time integral of the stress autocorrelation function. Let $\eta(t_{\max})$ be this value as a function of the truncation limit. To be accurate, this truncation has to be done at a value where the SACF is as close as possible to its zero long time limit value. The SACF fluctuates strongly around this value and an important computational effort is required to make it converge. The first and usual way to improve its convergence is to consider many time origins along the simulation run in the computation of the thermodynamic mean in the correlation function. In this study, we considered at least 290 000 time origins separated by 10 time steps from each other. As the liquid is isotropic, the second way is to average over three off-diagonal elements of the stress tensor σ_{xy}, σ_{yz}, σ_{xz}, and three directions obtained by 45° rotation of the axes [31], namely $\frac{1}{2}(\sigma_{xx} - \sigma_{yy})$, $\frac{1}{2}(\sigma_{yy} - \sigma_{zz})$, and $\frac{1}{2}(\sigma_{xx} - \sigma_{zz})$. In Fig. 4, we present typical curves of $\eta(t_{\max})$ as a function of $t_{\max}$ for eight
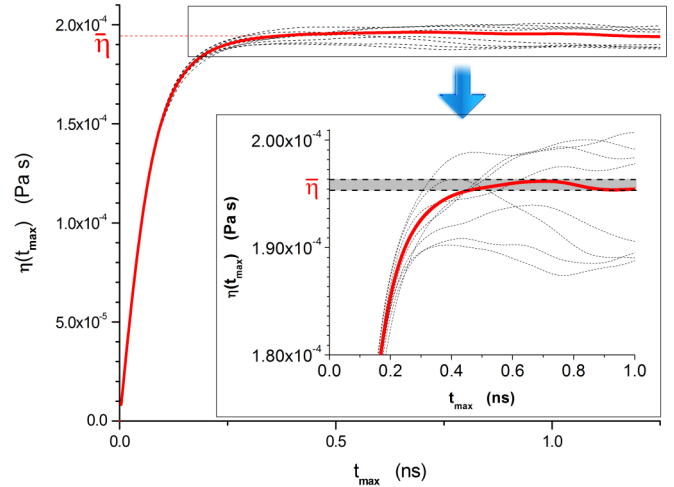
FIG. 4. Viscosity $\eta(t_{\max})$ as a function of truncation time $t_{\max}$. Think solid red curve corresponds to the average of 8 runs (thin dashed lines). Data are obtained at atmospheric pressure and $T = 770$ K.

runs (thin dashed lines) as well as the average of these curves (thick red curve). For a given state point, these eight runs were performed from the same initial configuration by increasing the thermalization stage from 55 000 to 85 000 steps in order to get 8 independent microscopic states corresponding to the same macroscopic state point. As can be seen from the figure, the curves obtained for each run are still fluctuating and it is not easy to locate accurately the asymptotic limit by considering a single curve. Depending on the investigated thermodynamic state, the fluctuations are more or less important. In the worst situation that we encountered, the dispersion between the single curves was about 10%. On the other hand, the mean of these eight curves converges nicely to an estimation of the shear viscosity value, $\bar{\eta}$. Thus, for each state point, we performed 8 runs obtained in the same way and we estimate the statistical uncertainty to be about 5%.

We checked the influence of the number of particles on the behavior of the SACF. No significant effect of N was observed, especially if $N \geqslant 1000$ as confirmed by several studies [28,31]. However, increasing the number of particles permits us to reduce the pressure and temperature fluctuations which scale as $N^{-1/2}$ during an NVE simulation [28]. Increasing the number of particles also has an effect on the behavior of $\eta(t_{\max})$. Indeed, $t_{\max}$ should be kept smaller than the time needed for a sound wave to cross the box. Otherwise, we observe a drift in $\eta(t_{\max})$ as $t_{\max}$ increases correlated with the periodic boundary conditions. Using $N = 2048$ allows us to reach the plateau in $\eta(t_{\max})$ before this effect appears.

III. RESULTS

In this section, we present our results for the shear viscosity of liquid sodium.

A. Comparison with experimental data

Before analyzing the influences of temperature and density, we compare our results with experimental data available in the literature in Fig. 5. These data were obtained under pressures
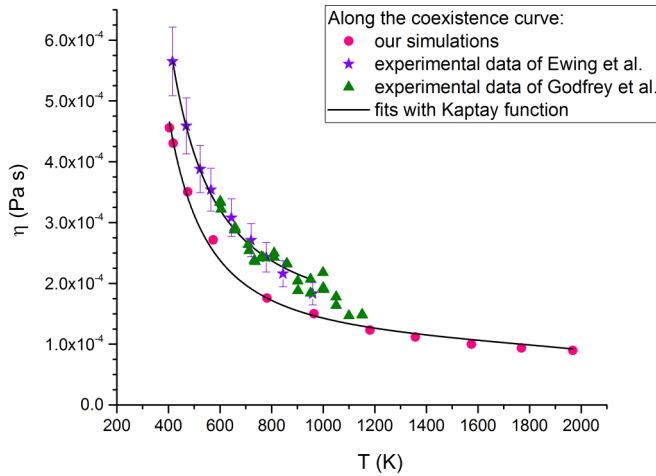
FIG. 5. Viscosity as a function of temperature along the liquid-gas coexistence border. Comparison between experimental (stars [8], triangles [32]) and our simulation data. Solid lines are fits obtained using Kaptay's expression.

close to the atmospheric one (as the sample was sealed into a container). Under normal pressure between melting and boiling points, the isobaric line is very close to the liquid-gas coexistence border. The simulation results were obtained along this coexistence line up to 2000 K. Data given by Ewing *et al.* [8] (stars) were presumably smoothed by these authors, in contrast to the results of Godfrey *et al.* [32] (triangles). Fluctuations in Godfrey *et al.* data are due to the low viscosity which makes accurate measurements difficult. Nevertheless, both experimental studies show similar results.

Comparing simulated and experimental shear viscosity, there clearly appears a shift between both sets of curves. The relative difference may seem rather high, but it should be considered that sodium viscosity is very low and the difference is in fact only about 4×10^{-5} Pa s. This difference may be due to inaccuracies in the description of the interactions. It should also be recalled that due to chemical reactivity of sodium, the viscosity is indirectly measured from the damping of the oscillations of a container filled with fluid. These measurements are very delicate and, surprisingly, date back to the 1960s for the most recent, to the best of our knowledge. Moreover, according to Kasama *et al.* [33], viscosity of liquid metals is very sensitive to impurities. For instance, the viscosity of Hg is increased 8% by the addition of 1 at. % of Ag. Similarly, adding 1 at. % of P or S divides iron viscosity by 2. Consequently, even if the pair potential is certainly the most important source of discrepancies, a need for updated experimental data of the viscosity of this metal is great.

On the other hand, notwithstanding the above-mentioned shift, our data nicely reproduce the variation of the viscosity along this line and we believe that they are appropriate to discuss temperature and density dependence of this physical quantity.

Kaptay [34] proposed an equation which is able to model the viscosity of pure liquid metals at their melting point and also its variation with temperature under normal pressure. Two competing concepts previously introduced to describe the temperature dependence of viscosity, namely activation energy

and free volume, have been unified and combined thanks to Andrade's equation [35] in order to elaborate the following relation:

$$\eta = A \frac{\rho^{2/3} T^{1/2}}{M^{1/6}} e^{BT_m/T}, \qquad (7)$$

where η, M, and T_m are viscosity, molar mass, and melting temperature of a given metal, respectively, ρ and T being the mass density and temperature at the considered state point. The semiempirical parameters A and B appeared to be nearly the same for all the metals considered.

In Fig. 5, we have also drawn the curves fitted to the experimental data of Ewing and to ours using Eq. (7). This relation reproduces nicely the behavior of the shear viscosity along the coexistence line even up to temperature as high as 2000 K. Of course, parameters A and B have different values for each data set: we obtain $A = 1.50 \times 10^{-8}$ [J$^{\frac{1}{2}}$ (K mol)$^{-\frac{1}{6}}$] and $B = 2.63$ for Ewing's data and $A = 1.01 \times 10^{-8}$ and $B = 2.78$ for our simulation data. The slight difference between both sets of parameters values is first due to the shift existing between both curves, but also to the temperature range on which the fit was performed. Indeed, experimental data of Ewing are known on a much smaller range [416–959 K] than our simulations performed over the [370–2000 K] interval. If we restrict the fit of the simulation data to the same temperature range, we obtain $A = 1.125 \times 10^{-8}$ and $B = 2.66$. Consequently, Kaptay's relation seems to model correctly the behavior of the viscosity along the liquid-vapor coexistence curve.

However, there is an implicit dependence between temperature and density along this line and it appears that this expression is not able to separately take into account density and temperature dependence. In Fig. 6, we have plotted our results along an isochoric line and tried to fit them using Eq. (7). It appears that this relation does not properly reproduce the evolution of the viscosity over a large temperature range.
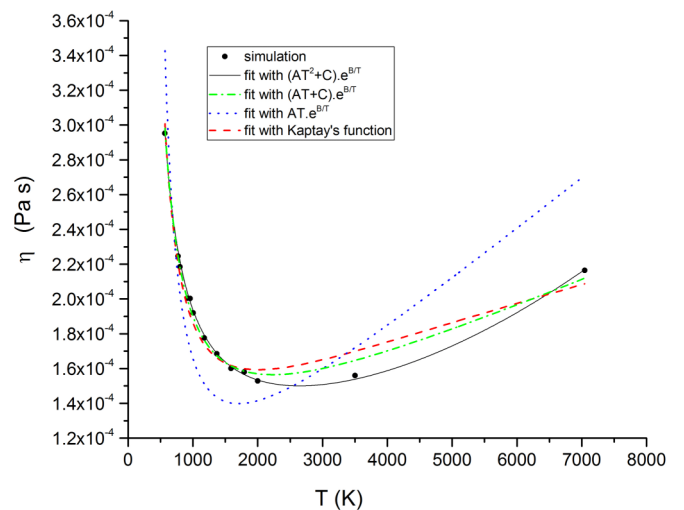
FIG. 6. Viscosity as a function of temperature along the isochoric line $\rho = 900 \, \text{kg m}^{-3}$. Symbols are simulation results. Red dashed line corresponds to the fit with Kaptay function, while black solid line is the fit with the expression proposed in Eq. (8). Green dash-dotted and blue dotted curves correspond to other expressions discussed in the text.

In fact, the validity of this relation is limited to a specific range of the phase diagram, namely close to the melting point and under relatively low pressures. According to Kaptay, the validity of the expression is limited to pressures lower than 100 bars, i.e., close to the liquid-gas coexistence. Within the scope of our study, the pressures are much higher than this limit (at a density of 2000 kg m^{-3}, the pressure is about 0.2 Mbar). Equation (7) also does not correctly reproduce the very low density behavior. Along an isotherm, if density tends to zero, this function tends to zero. However, according to the Chapman-Enskog solution of the Boltzmann equation [35], the viscosity must tend to a finite constant.

Thus, Kaptay's relation can only be applied in a very limited region of the phase diagram and around the liquid-gas coexistence. In the following, we propose a relation that permits us to separately study the influence of temperature and density on the viscosity and that is valid in a large region covering the liquid state.

B. Temperature dependence

The shear viscosity of sodium is shown in Fig. 7 as a function of temperature. Nine isochoric lines are plotted corresponding to state points represented in Fig. 2. At $\rho \geqslant 900$ kg m^{-3} the curves have the same typical behavior: as temperature increases, viscosity decreases quickly at low temperatures, reaches a minimum, and increases slowly in the high-temperature region.

Such a qualitative behavior is expected from the asymptotic behaviors of Kaptay's relation and confirmed by experimental measurements [36] on argon. As explained by Meier *et al.* [37], it results from the interplay between three contributions to viscosity (kinetic-kinetic η_{kk}, kinetic-potential η_{kp}, and potential-potential η_{pp} terms). They showed

that η_{pp} (which quickly decreases with T) dominates at high densities, contrary to the gas region where η_{kk} (which slowly increases with T) is the largest contribution to the viscosity.

At low densities, where the interaction contribution becomes negligible, the kinetic part increasing with temperature prevails. Even if we could not reach too low densities due to the metal-to-nonmetal transition, this is clearly recovered at the lowest density displayed ($\rho = 637$ kg m^{-3}) whose curve is parallel to the zero-density viscosity η_0. These limiting values were determined from a linear function developed on the basis of several low-density data [38–40] and proposed by Verfaftik *et al.* in Ref. [27] (Chap. 7.3, p. 822). The same slope is observed between both curves indicating how, at low densities, the viscosity depends on the temperature. Compared to η_0, the shift shows the density dependence.

At higher densities, this kinetic contribution still dominates, provided that the temperature is high enough. On the other hand, at low temperatures, the potential contribution due to the interatomic interactions prevails. As this contribution decreases with T, an increase of the temperature leads to a fast decrease of the viscosity. This is a rather intuitive behavior if one considers that the increase of temperature leads to a raising of thermal excitation that hinders cohesion of the material.

Thus, except for the lower densities, a minimum in the viscosity is found for each isochoric line. In Fig. 7, they are indicated by stars that are located on the red dotted curve. In the work of Meier *et al.* [37] on the Lennard-Jones fluid (see inset in Fig. 7), the same behavior was observed along isochoric lines. However, Meier's data suggest that a minimum no longer exists at the highest densities. As they were limited to rather low temperatures, we have performed some simulations of Lennard-Jones fluids at $\rho^* = 0.95$ and temperatures up to $T^* = 10$. The viscosity values that we obtained are identical in the temperature range they studied (confirming if necessary that our calculations of the viscosity by the Green-Kubo method are correct). Moreover, a minimum is observed even at the highest density, provided that the temperature range is wide enough. Thus, the occurrence of a minimum in the temperature dependence of the viscosity at constant density seems to be a general feature exhibited by both metallic and rare gas fluids at liquid densities.

As we mentioned above, Kaptay's relation qualitatively reproduces the temperature dependence of viscosity, but it is not satisfactory on a quantitative point of view (see Fig. 6). This is also observed in the case of the Lennard-Jones fluid. This is partly due to the fact that part of the temperature dependence is implicitly included in the density term as it varies with T. Moreover, Kaptay's relation has been developed for a limited temperature range and it is not surprising that its extrapolation fails in reproducing the data. The discrepancy mainly concerns the high-temperature part of the curves where the $T^{1/2}$ term seems to be unsatisfactory. Let us consider the Stokes-Einstein relation which will be discussed in detail in Sec. III D. According to this relation, η is proportional to T/D, with D the self-diffusion coefficient. On restricted temperature ranges, the temperature dependence of D is often depicted as an Arrhenius law, $A \exp(-B/T)$. Thus, a first guess could be to consider the following relation: $AT \exp(B/T)$. In fact, it also appears to be unsatisfactory (see Fig. 6). This has to be
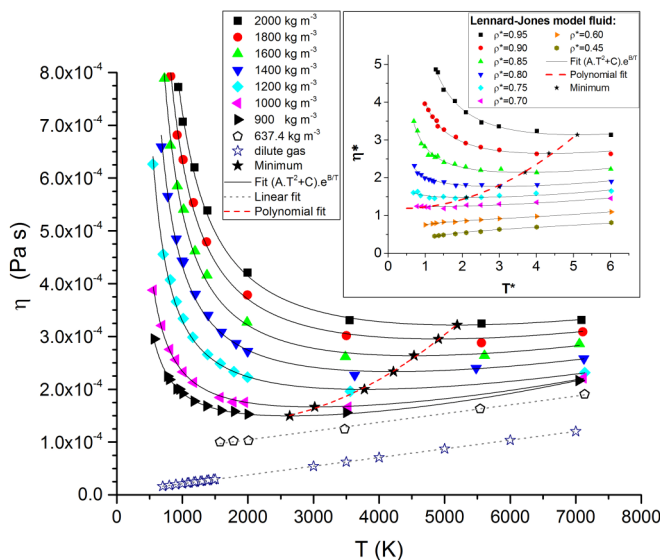
FIG. 7. Viscosity of sodium, η, as a function of temperature for different isochoric lines. Black solid lines correspond to the fitting by the relation proposed in Eq. (8). The minimum of each fit is pointed out by stars located on the red dotted line. Inset: Same study for Lennard-Jones model fluid as done by Meier *et al.* [37] and completed by us. Same color code and symbol are used.
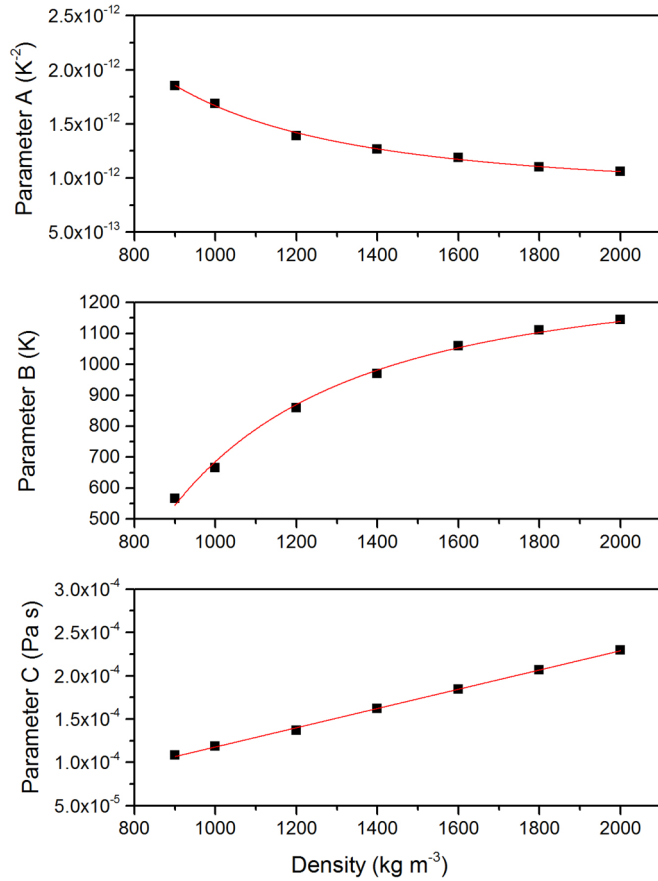
FIG. 8. Parameters A, B, C as functions of the density ρ. Red solid lines correspond to fit of the data as described in the text.

related to the known deviation of the $D = D(T)$ dependence from an Arrhenius law [16].

Having tried several expressions involving a limited number of adjustable parameters, we noticed that the best agreement was obtained over the whole density domain with the following expression:

$$\eta(T) = (AT^2 + C)e^{B/T}, \tag{8}$$

where A, B, and C are parameters depending on the density. As seen in Fig. 7, this function reproduces both qualitatively and quantitatively the temperature dependence of the viscosity of sodium as well as that of the Lennard-Jones fluid (see inset). Asymptotic behaviors are well accounted for in both the low and high density limits of the investigated temperature interval. We did not succeed in finding phenomenological or theoretical justification for this expression and we guess that this point could stimulate further research.

Each isochoric line was fitted by this new function and parameters A, B, and C are plotted as functions of density in Fig. 8. Such a smooth behavior of the fitting parameters with density leads us to believe that the agreement between simulation data and fitting function could be not fortuitous.

The parameter C has a linear behavior

$$C = \alpha_C + \beta_C \rho, \tag{9}$$

TABLE I. Parameter values of Eqs. (9), (10), and (11).

	$A(\mathrm{K}^{-2})$	B (K)	C (Pa s)
α	8.12×10^{-7}	-6.03×10^{8}	6.56×10^{-6}
β	8.54×10^{-13}	1.289×10^{3}	1.11×10^{-7}

whereas both A and B are modeled by

$$A = \frac{\alpha_A}{\rho^2} + \beta_A, \tag{10}$$

$$B = \frac{\alpha_B}{\rho^2} + \beta_B. \tag{11}$$

The values of the parameters are summarized in Table I.

C. Density dependence

Replacing parameters A, B, and C by their expressions in Eq. (8) and rearranging it, we obtain a relation which depends simultaneously on temperature and density:

$$\eta(\rho,T) = \left[\left(\frac{\alpha_A}{\rho^2} + \beta_A\right)T^2 + (\alpha_C + \beta_C\rho)\right]e^{(\frac{\alpha_B}{\rho^2} + \beta_B)/T}. \tag{12}$$

In Fig. 9, shear viscosity is plotted as a function of density along ten isotherms. Viscosity increases with density. This is rather intuitive since increasing density implies that the particles are getting closer to each other, leading to an increase of collisions and, consequently, of viscosity. A linear behavior in the high-density range of each isotherm can also be noticed.

Since viscosity values at low density are not accessible below the metal-to-nonmetal transition ($\rho < 2.5\rho_c$), it is difficult to have a clear picture of the density dependence below this limit. However, the behavior of viscosity below 1000 kg m^{-3} seems to depart from linearity. This is consistent
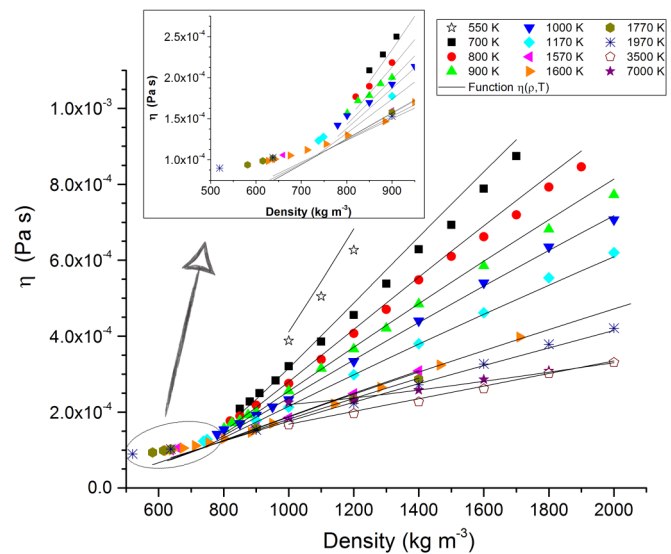
FIG. 9. Viscosity, η, of sodium as a function of density, ρ, along different isotherms. Symbols: Simulation results; black lines: results of Eq. (12) with parameters of Table I. Inset: Same plot, but for densities lower than 900 kg m^{-3}.

with the fact that viscosity must tend to a nonzero constant at zero density according to the Chapman-Enskog theory.

In order to clarify this tendency, we can consider the study of Meier *et al.* [37] on the Lennard-Jones fluid. In this system, there appears a transition between high and low density regimes. At low densities, the viscosity tends to a constant whereas at high densities, it increases sharply and seems to follow a linear law (this last point is difficult to confirm from their original figure). At intermediate densities (about $2\rho_c$–$2.5\rho_c$), isotherm curves intersect and this is recovered in our results for sodium. But, in our case, this range is difficult to highlight as we are limited by both liquid-vapor and metal-to-nonmetal transitions. Below the crossing point, viscosity increases with temperature while it decreases at densities above this point, in full consistency with our results displayed in the previous section.

In Fig. 9, we have also drawn the curves obtained from Eq. (12) using parameter values deduced from the fit of isochoric lines and summarized in Table I. We first observe that viscosity values along isotherms predicted by this equation are in good agreement with our simulation data, except at the smallest densities. The discrepancies are due to a wrong asymptotic limit of this function which should tend to a nonzero value as the density tends to zero as we mentioned above. Indeed, if T is kept constant, Eq. (12) can be rewritten as

$$\eta(\rho) = \left(\frac{a}{\rho^2} + b + c\rho\right)e^{d/\rho^2}. \tag{13}$$

This equation is numerically consistent with a linear behavior of isotherms at high densities, but does not tend to a finite constant as the density tends to zero (here, $d < 0$).

Once again, this has to be attributed to the fact that we cannot investigate the low-density part of the phase diagram, so that our expressions of the density dependence of the parameters A, B, and C should not be extrapolated to this limit. However, with parameter values of Table I, Eq. (12) reproduces qualitatively and quantitatively well the viscosity of liquid sodium at any temperature between 700 and 7000 K (corresponding to $[0.28T_c, 2.8T_c]$) and any density between 900 and 2000 kg m^{-3} (corresponding to $[3.9\rho_c, 8.7\rho_c]$).

D. Stokes-Einstein relation

The well-known Stokes-Einstein (S-E) relation [41] relates two fundamental dynamic properties, the diffusion coefficient (D) of a particle and the viscosity (η) of the liquid. For a Brownian particle in a solvent, it states

$$D = \frac{k_B T}{C\pi\eta R}, \tag{14}$$

where $C = 6$ for the slip boundary condition, and $C = 4$ for the stick boundary condition [30], and R is the radius of the particle. In a dense fluid, this equation is found to be quite valid, when an appropriate definition of R (now called the hydrodynamic radius [30]) is taken, and with the constant C depending on the liquid considered [41]. An approximate theoretical investigation [41] suggests that with R being the so-called Wigner-Seitz radius

$$R_{WS} = (3/4\pi n)^{1/3}, \tag{15}$$

$n = N/V$ being the number density, Eq. (14) becomes

$$D = \frac{k_B T}{4\pi\eta R_{WS}}. \tag{16}$$

Another theoretical proposition also suggests R_{WS} for the radius, but gives $C = 3$ for dense liquids [42,43]. Tests done on Lennard-Jones liquids give $C = 3.1$, very close to 3 [41,44]. On the other hand, for a hard-sphere fluid, predictions based on the Enskog kinetic theory indicate C depending slightly on the volume fraction, in the range $3.2 < C < 4.8$ [44]. Here we check this relation for liquid sodium, in the wide region of the phase diagram explored. Besides R_{WS}, we also explore two other possibilities for R, namely $R_1 = r_{\min}/2$, or $R_2 = r_{\max}/2$, with $r_{\min}$ the distance at which $g(r)$ takes off from 0, and $r_{\max}$ the location of its main peak.

The diffusion coefficient (D) is obtained from the mean-squared displacement of the atoms. Unlike the viscosity, D depends on the system size [45]; the corrected expression for D is

$$D = D_{PBC} + 2.837k_B T n^{1/3}/(6\pi\eta N^{1/3}), \tag{17}$$

where D_{PBC} is the finite-size diffusion coefficient (using the periodic boundary conditions). We rewrite Eq. (14) as

$$C = \frac{k_B T}{\pi\eta R_{WS}D}, \tag{18}$$

and we investigate the values of C obtained from different hypothesis for R, using D_{PBC} and the corrected D.

Our results are gathered in Fig. 10. Panel (a) shows the C values vs T along the liquid-gas coexistence line. We can see that using $R = R_{WS}$ and the corrected D, we obtain C values which are relatively constant, and included in the range $3.5 < C < 4.7$. There is a slight tendency for C to increase with T, but this increase is not strong (not exceeding 1.2). The other hypotheses for R, on the other hand, seem to predict C values that are too large compared to the known values for the Lennard-Jones dense liquids. Furthermore, criteria based on $g(r)$ are less handy than the one based on n, for a given system.

Panel (b) displays C values vs T obtained along an isochoric line ($\rho = 900$ kg/m^3). This time again, using $R = R_{WS}$ and corrected D, we obtain C values which are stable, with C about 3.5.

In panel (c) is shown C vs ρ for one isotherm ($T = 700$ K). Except the first few points, C is remarkably stable and is about 3.3 for a relatively large range of density ($1000 < \rho < 1800$ kg/m^3).

In conclusion, our investigation on the S-E relation indicates that such a relation, although not rigorously valid in dense liquid sodium, is however semiquantitatively correct. More precisely, if we adopt the Wigner-Seitz radius for the hydrodynamic radius, using a value of $C = 3.6$, we can obtain the diffusion coefficient D within about 30% error, knowing η and using the S-E relation Eq. (14).

Thus, this relation can be quite useful for experimentalists investigating these liquids as viscosity is easier to measure than the diffusion coefficient, but also conversely for simulations as the diffusion coefficient can easily be computed.
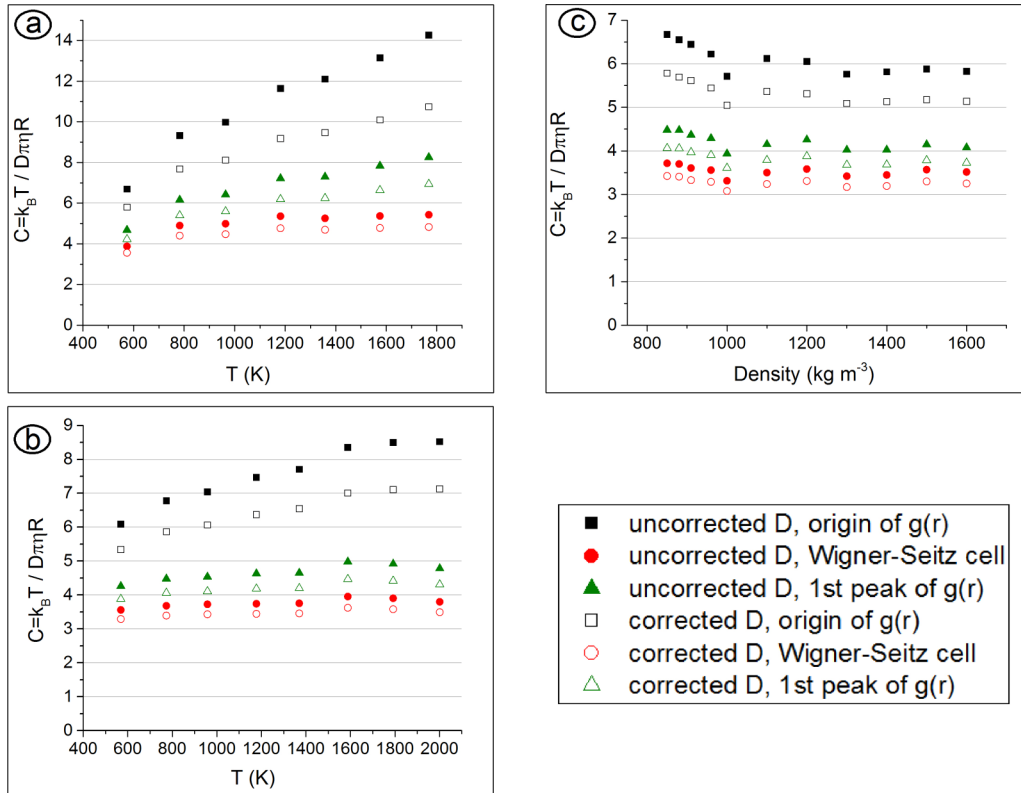
FIG. 10. Parameter C vs T along the liquid-gas coexistence line (a); vs T along the isochoric line $\rho = 900$ kg/m^3) (b); vs ρ along the isotherm $T = 700$ K (c).

IV. CONCLUSION

In this study, we have applied equilibrium molecular dynamics simulations to the study of viscosity of liquid sodium over a wide range of the phase diagram. We estimate the statistical accuracy of our results to 5%. Close to the liquid-gas coexistence, they fairly well agree with experimental data. The accuracy of the description of the interactions is surely the main cause of the difference. Nevertheless, the need for updated experimental data is patent.

Along isochoric lines, viscosity presents a minimum as temperature increases, except at the lowest densities investigated. On the other hand, it monotonically increases along isotherms. While Kaptay's relation satisfactorily describes the evolution of viscosity along the liquid-vapor coexistence curve, it fails to disentangle temperature and density influences. Therefore, we proposed a relation which, in the investigated range, qualitatively and quantitatively describes the viscosity of liquid sodium.

Interestingly, the same qualitative behavior has been reported for the Lennard-Jones fluid and the relation proposed in this study seems also able to describe the viscosity of rare gas fluids. Universal behaviors of many physical properties of liquid alkali metals have already been reported. It could be interesting to further extend the study of the influence of temperature and density on the viscosity to other fluids, especially metallic ones, because of their potential practical use.

Finally, we also investigated the validity of the Stokes-Einstein relation. We observed that it applies to liquid sodium within 30% accuracy with $C = 3.6$ provided that the Wigner-Seitz radius is used as the effective hydrodynamic radius.

ACKNOWLEDGMENT

[1] M. L. Rudolph, V. Lekić, and C. Lithgow-Bertelloni, Science **350**, 1349 (2015).

[2] M. Berhanu, R. Monchaux, S. Fauve, N. Mordant, F. Pétrélis, A. Chiffaudel, F. Daviaud, B. Dubrulle, L. Marié, F. Ravelet, M. Bourgoin, P. Odier, J.-F. Pinton, and R. Volk, Europhys. Lett. **77**, 59001 (2007).

[3] J. P. Poirier, Geophys. J. **92**, 99 (1988).

[4] D. E. Smylie, V. V. Brazhkin, and A. Palmer, Phys. Usp. **52**, 79 (2009).

[5] D. Alfè, G. Kresse, and M. J. Gillan, Phys. Rev. B **61**, 132 (2000).

[6] M. D. Dickey, R. C. Chiechi, R. J. Larsen, E. A. Weiss, D. A. Weitz, and G. M. Whitesides, Adv. Funct. Mater. **18**, 1097 (2008).

[7] V. Sobolev, Scientific Report of the Belgian Nuclear Research Centre, SCK-CEN-BLG 1069, 2011.

[8] C. T. Ewing, J. A. Grand, and R. R. Miller, J. Phys. Chem. **58**, 1086 (1954).

[9] I. I. Novikov, A. N. Soloviev, E. M. Khabakhnasheva, V. A. Gruzdev, A. I. Pridantzev, and M. Ya. Vasenina, J. Nucl. Energy **4**, 387 (1957).

[10] E. E. Shpilrain, Y. A. Soldatenko, K. A. Yakimovich, V. A. Fomin, V. A. Savchenko, A. M. Belova, D. N. Kagan, and I. F. Krainova, High Temp. **3**, 930 (1965).

[11] Y. S. Chiong, Proc. R. Soc. London A **157**, 264 (1936).

[12] J. Cheng, J. Gröbner, N. Hort, K. U. Kainer, and R. Schmid-Fetzer, Meas. Sci. Technol. **25**, 062001 (2014).

[13] L. M. Berezhkovsky, A. N. Drozdov, V. Yu Zitserman, A. N. Lagar'kov, and S. A. Triger, J. Phys. F **14**, 2315 (1984).

[14] T. Koishi, Y. Shirakawa, and S. Tamaki, Comput. Mater. Sci. **6**, 245 (1996).

[15] C. Fiolhais, J. P. Perdew, S. Q. Armster, J. M. MacLaren, and M. Brajczewska, Phys. Rev. B **51**, 14001 (1995); **53**, 13193(E) (1996).

[16] J.-F. Wax, R. Albaki, and J.-L. Bretonnet, Phys. Rev. B **65**, 014301 (2001).

[17] J.-F. Wax and N. Jakse, Phys. Rev. B **75**, 024204 (2007).

[18] J.-F. Wax, Physica B **403**, 4241 (2008).

[19] J.-F. Wax and T. Bryk, J. Phys.: Condens. Matter **25**, 325104 (2013).

[20] S. Ichimaru and K. Utsumi, Phys. Rev. B **24**, 7385 (1981).

[21] A. Yamane, F. Shimojo, and K. Hoshino, J. Phys.: Conf. Ser. **98**, 012024 (2008).

[22] J.-Y. Raty, E. Schwegler, and S. A. Bonev, Nature (London) **449**, 448 (2007).

[23] G. H. Golden and J. V. Tokar, AEC Research and Development Report, ANL 7323, 1967.

[24] J. B Neaton and N. W. Ashcroft, Phys. Rev. Lett. **86**, 2830 (2001).

[25] M. Hanfland, I. Loa, and K. Syassen, Phys. Rev. B **65**, 184109 (2002).

[26] L-D. Lucas, Techniques de l'ingénieur: Matériaux métalliques **M65** (1984).

[27] R. W. Ohse, *Handbook of Thermodynamic and Transport Properties of Alkali Metals* (Blackwell, Oxford, 1985).

[28] D. Nevins and J. Spera, Mol. Simul. **33**, 1261 (2007).

[29] M. P. Allen and D. J. Tildesley, *Computer Simulation of Liquids* (Oxford University Press, New York, 1989).

[30] J.-P. Hansen and I. R. McDonald, *Theory of Simple Liquids*, 2nd ed. (Academic Press, San Diego, 1986).

[31] B. L. Holian and D. J. Evans, J. Chem. Phys. **78**, 5147 (1983).

[32] G. W. Thomson and E. Garelis, in *Physical and Thermodynamic Properties of Sodium*, ACS Monograph Series, No. 133 (Reinhold Pub. Corp., New York, 1956), p. 12.

[33] A. Kasama, T. Iida, and Z.-I. Morita, Trans. Jpn. Inst. Met. **16**, 527 (1975).

[34] G. Kaptay, Z. Metallkd. **96**, 24 (2005).

[35] E. N. Andrade, Philos. Mag. **17**, 497 (1934).

[36] R. Vogelsang and C. Hoheisel, Phys. Chem. Liq. **18**, 141 (1988).

[37] K. Meier, A. Laesecke, and S. Kabelac, J. Chem. Phys. **121**, 3671 (2004).

[38] B. I. Stefanov, D. L. Timrot, E. E. Totsky, and Chu Ven-Hao, Teplofiz. Vys. Temp. **4**, 141 (1966).

[39] D. L. Timrot and A. N. Varava, Teplofiz. Vys. Temp. **15**, 750 (1977).

[40] N. I. Sidorov, Y. V. Tarlakov, and V. S. Yargin, Izv. VUZov. Energetica **11**, 93 (1976).

[41] U. Balucani and M. Zoppi, *Dynamics of the Liquid State* (Clarendon, Oxford, 1994).

[42] H. Eyring and T. Ree, Proc. Natl. Acad. Sci. USA **47**, 526 (1961).

[43] R. Zwanzig, J. Chem. Phys. **79**, 4507 (1983).

[44] N. Ohtori and Y. Ishii, Phys. Rev. E **91**, 012111 (2015).

[45] I.-C. Yeh and G. Hummerl, J. Phys. Chem. B **108**, 15873 (2004).